Poultry Science®

Selenium represses microRNA-202-5p/MICU1 aixs to attenuate mercuric chloride-induced kidney ferroptosis

Yue Li,[*,†,‡] Han Cui,[*,†,‡] Wan-Xue Xu,[*,†,‡] Hong-Yu Fu,[*,†,‡] Jiu-Zhi Li,[*,†,‡] and Rui-Feng Fan[*,†,‡,1]

[*]*College of Veterinary Medicine, Shandong Agricultural University, Tai'an City, Shandong Province, 271018, China;* [†]*Shandong Provincial Key Laboratory of Animal Biotechnology and Disease Control and Prevention, Shandong Agricultural University, Tai'an City, Shandong Province, 271018, China; and* [‡]*Shandong Provincial Engineering Technology Research Center of Animal Disease Control and Prevention, Shandong Agricultural University, Tai'an City, Shandong Province, 271018, China*

ABSTRACT Mercuric chloride (**$HgCl_2$**) is a nephrotoxic contaminant that is widely present in the environment. Selenium (**Se**) can effectively antagonize the biological toxicity caused by heavy metals. Here, in vivo and in vitro models of Se antagonism to $HgCl_2$-induced nephrotoxicity in chickens were established, with the aim of exploring the specific mechanism. Morphological observation and kidney function analysis showed that Se alleviated $HgCl_2$-induced kidney tissue injury and cytotoxicity. The results showed that ferroptosis was the primary mechanism for the toxicity of $HgCl_2$, as indicated by iron overload and lipid peroxidation. On the one hand, Se significantly prevented $HgCl_2$-induced iron overload. On the other hand, Se alleviated the intracellular reactive oxygen species (**ROS**) levels caused by $HgCl_2$. Subsequently, we focused on the sources of ROS during $HgCl_2$-induced ferroptosis. Mechanically, Se reduced ROS overproduction induced by $HgCl_2$ through mitochondrial calcium uniporter (**MCU**)/mitochondrial calcium uptake 1 (**MICU1**)-mediated mitochondrial calcium ion (**Ca^{2+}**) overload. Furthermore, a dual luciferase reporter assay demonstrated that MICU1 was the direct target of miR-202-5p. Overall, Se represses miR-202-5p/MICU1 axis to attenuate $HgCl_2$-induced kidney ferroptosis.

Key words: selenium, mercuric chloride, mitochondrial calcium overload, MicroRNA-202-5p/MICU1 axis, ferroptosis

2024 Poultry Science 103:103891
https://doi.org/10.1016/j.psj.2024.103891

INTRODUCTION

Mercury (**Hg**) is a highly toxic environmental pollutant, and in recent years Hg pollution has become an increasingly prominent problem (Chen et al., 2022a). In the nature, Hg exists as monomeric Hg, organic Hg, and inorganic Hg (Caglayan et al., 2019). Mercuric chloride (**$HgCl_2$**), as a widely distributed inorganic Hg, is used mainly in industrial and agricultural production and daily life, such as gold mining, light bulb, and skin-lightening cosmetics. $HgCl_2$ is accumulated in the environment, and further enters the food chain, where it is enriched in animals and humans, causing harmful effects on several organs, including the kidney (Ma et al., 2018), testis (Chen et al., 2022b), and liver (Hazelhoff and Torres, 2018). $HgCl_2$ is mainly absorbed and accumulated in the kidney, therefore the kidney is the main target organ in which $HgCl_2$ exerts toxicity. Previous studies on $HgCl_2$-induced nephrotoxicity have focused mainly on apoptosis (Fan et al., 2020), necrosis (Hosseini et al., 2018), and autophagy (Avila-Rojas et al., 2019), while few reports have been reported on emerging modes of cell death, especially ferroptosis.

Ferroptosis is a new type of programmed cell death that is distinct from apoptosis, necrosis, and autophagy, which is mainly characterized by elevated intracellular ferrous iron (**Fe^{2+}**) levels and accumulated lipid peroxides (Dixon et al., 2012). Intracellular iron homeostasis relies on the coordination of iron absorption, export, storage, and utilization (Hao et al., 2018). In the physiological state, transferrin receptor (**TFRC**) delivers ferric ion (**Fe^{3+}**) into cells, and ferroportin (**FPN**) transports Fe^{2+} outside the cells. Free iron that enters the cells is stored in a complex composed of ferritin heavy chain 1 (**FTH1**) (Fuhrmann, et al., 2020). Especially, iron response element binding protein 2 (**IREB2**), an iron sensor participating in cellular iron regulation, maintains iron homeostasis by regulating gene expression related to iron metabolism (including FTH1, FPN1, and

Received March 19, 2024.
Accepted May 20, 2024.

[1]Corresponding author: fanruifeng@sdau.edu.cn

TFRC) (Dixon et al., 2012). Meanwhile, IREB2 is bound and degraded during intracellular iron overload by F-box and leucine-rich repeat protein 5 (**FBXL5**), which reduces iron uptake and promotes iron storage and export (Wang et al., 2020). It is noteworthy that iron overload caused by intracellular iron disorders generates reactive oxygen species (**ROS**) via the iron-dependent Fenton reaction, an essential trigger of ferroptosis (Latunde-Dada, 2017). More importantly, our group has proven that $HgCl_2$ induced intracellular iron overload in chicken embryo kidney (**CEK**) cells through ferritinophagy and led to a continuous accumulation of ROS, triggering ferroptosis (Chu et al., 2022). Furthermore, arsenic has been reported to cause mitochondrial ROS accumulation and lead to ferroptosis in a manner that is not dependent on iron metabolism imbalance (Li et al., 2022b). Therefore, the source of ROS needs to be further explored.

Mitochondria are considered the prominent organelle for ROS production, and a change in mitochondrial metabolic function can produce excessive ROS (Yang et al., 2021). Interestingly, calcium ion ($\mathbf{Ca^{2+}}$) is a well-known second messenger and a key regulator of mitochondrial function (Bravo-Sagua et al., 2017). Mitochondrial calcium uptake 1 (**MICU1**) is a soluble protein in the inner mitochondrial membrane according to Ca^{2+} concentration on both sides of the mitochondria that interacts directly with mitochondrial calcium uniporter (**MCU**) and regulates channel activity (Paupe and Prudent, 2018). Available evidence suggested that MICU1 deficiency contributed to mitochondrial Ca^{2+} overload and subsequently excessive ROS production (Yang et al., 2020). Crucially, $HgCl_2$ has been shown to cause an imbalance in cellular Ca^{2+} entry and exit, leading to kidney Ca^{2+} overload in mice (Li et al., 2019b). Therefore, it was wondered whether the disrupted interaction between MCU and MICU1 is a checkpoint for $HgCl_2$-induced mitochondrial Ca^{2+} overload and further contributes to the appearance of ROS-dependent ferroptosis.

MicroRNAs (**miRNA**) are a group of single-stranded noncoding RNA molecules that primarily regulate the transcription and expression of biologically active genes. MiRNAs play major roles in many physiological and pathological processes, and there is evidence suggested that miRNAs are essential in cell death (Bao et al., 2020). Previous studies have demonstrated that environmental toxicants such as cadmium (**Cd**) and Hg can alter epigenetic regulatory features such as miRNAs expression patterns in rats and humans (Ding et al., 2017; Liang et al., 2021). Furthermore, MCU was determined to be a direct target of miR-25, and the overexpression of miR-25 reduced mitochondrial Ca^{2+} overload in mouse cardiomyocytes (Hu et al., 2022). In addition, there is clear evidence that ischemia/reperfusion caused kidney ferroptosis in rats by mediating upregulation of miR-378-3p and miR-182-5p, directly targeting solute carrier family 7 member 11 and glutathione peroxidase 4 (**GPX4**) (Ding et al., 2020). Besides, miR-302 was found to target and inhibit MICU1 expression in type 2 lung alveolar cells (Ali et al., 2022). However, it is still elusive whether miRNAs cause Ca^{2+} overload in chicken kidney by targeting MICU1.

Selenium (**Se**) plays essential roles in animal organism and has a protective effect against cellular oxidative damage. Importantly, the functional importance of Se in ferroptosis has been widely demonstrated. For example, GPX4 is an essential selenoprotein with resistance to ferroptosis (Zhang et al., 2021). Furthermore, Se can antagonize Hg-induced organ toxicity by regulating selenoprotein expression and Hg-Se complex formation (Chu et al., 2020). Previous studies showed that Se deficiency disrupted Ca^{2+} homeostasis and triggered ROS overload in the swine small intestine, suggesting that Se was involved in the regulation of Ca^{2+} in vivo (Zheng et al., 2021). In particular, recent research also proved that Se reversely regulated Cd-triggered necrosis and apoptosis induced by miR-216a/PI3K/AKT axis (Zhang et al., 2020b). Therefore, this study hypothesized that Se could affect Ca^{2+} homeostasis through endogenous regulation, and thus inhibit $HgCl_2$-induced ferroptosis, which might involve the regulation of miRNAs.

MATERIALS AND METHODS

Animals and Treatments

All animal experiments were in accordance with the guidelines for the Care and Use of Laboratory Animals in Shandong Agricultural University (NO: SDAUA-2022-26). Sodium selenite ($\mathbf{Na_2SeO_3}$) and $HgCl_2$ were acquired from Sigma-Aldrich (Carlsbad, CA). Ninety male Hyline brown chickens (17-day-old, Dongyuezhongqin Co. Ltd., Tai'an, China) were randomly divided into 3 groups, including control (**Con**) group, $HgCl_2$ group, and $HgCl_2$ + Se group. All chickens adapted to the laboratory environment for 1 wk. Con group were received normal drinking water and standard diet, $HgCl_2$ group were received drinking water with 250 mg/L $HgCl_2$ and standard diet, and $HgCl_2$ + Se group were received drinking water with 250 mg/L $HgCl_2$ and standard diet with 10 mg/kg Na_2SeO_3 (Zhou et al., 2020). The chickens were euthanized after 7 wk of feeding. Cardiac puncture blood was collected for biochemical analysis. After removing kidney tissues, one part was fixed with 4% formaldehyde to make tissue sections, one part was ground into homogenate for the kit assay, and the remaining kidney tissues were stored at -80°C for further experiments.

Cell Cultures and Treatments

Briefly, embryos of 17-day-old Hyland Brown chickens (Dongyuezhongqin Co. Ltd., Tai'an, China) were taken out on the clean bench. The kidney tissues were removed using heat-sterilized forceps and scissors. The kidney tissues were washed with PBS, then cut and added trypsin for digestion, and digestion was terminated by adding an equal amount with 10% fetal bovine serum (Gibco, Waltham, MA) in M199 medium. After filtering and adding to a centrifuge tube, the

supernatant was then discarded, the medium was added and resuspended, and the plate was finally diluted for counting.

Histopathological Observation

Kidney tissues were fixed in 4% formaldehyde solution and embedded in paraffin wax. Fixed sections were placed at different concentrations (70−100%) of ethanol solution. Then dewax with xylene and deionized water. Sections were stained with hematoxylin and eosin (**H&E**), and then dehydrated. Finally, sections were fixed with neutral resin, and histopathological changes in the kidney were observed under a light microscope (Nikon Eclipse E600 W, Suzhou, China).

Cell Viability Assay

CEK cells were grown in 96-well plates at 4.5×10^4 cells per well overnight at 37°C. After the cells have fully adhered and grown to 80% confluence, the culture medium was removed and replaced with the culture medium containing different concentrations of Se (0, 1, and 10 μM). After 12 h with $HgCl_2$ (15 μM) treatment (Chu et al., 2022), the medium was replaced with 100 μL of fresh medium containing 10 μL of Cell Counting Kit-8 solution (**CCK-8**, Saint-Bio, Shanghai, China), and the cells were cultured for another 1 h at 37°C. The absorption of cell solution was measured at 490 nm.

Biochemical Analysis of Blood

Blood samples were taken in vacuum tubes, and serum biochemical indexes were detected using an automatic hematologic biochemical analyzer BC-2600 Vet (Mindray, Shenzhen, China).

Hoechst 33342/Propidium Iodide Staining

CEK cells under different treatments were incubated for 12 h at 37°C and the cells washed with PBS for 3 times. Subsequently, 1 mL cell staining buffer was added, and 5 μL Hoechst 33342 staining solution and 5 μL PI staining solution (Beyotime Biotechnology., Shanghai, China) were added at the same time with 4°C for 30 min in dark. After 3 washes with PBS, the dye mixture was discarded, and the cells were observed under a fluorescence microscope (Leica TCS SPE, Wetzlar, Germany).

Redox State Detection

Freshly collected kidney tissues were ground into a homogenate. After centrifugation at 3,500 × g for 10 min, the supernatant was transferred to a new tube. The commercial test kits obtained from Nanjing Jiancheng Bioengineering Institute (Nanjing, China) were used to measure the content of malondialdehyde (**MDA**), and the activities of total superoxide dismutase (**T-SOD**) and glutathione peroxidase (**GSH-Px**).

Determination of Lipid Peroxidation Biomarkers

After $HgCl_2$ and Se treatment, the medium was discarded, and CEK cells were transferred to a new centrifuge tube. Subsequently, the reagent was added to the centrifuge tube and incubated at 95°C for 40 min. After cooling, the centrifuge tube was kept at 4,000 × g for 10 min. Using a microplate reader to measure the absorbance at 532 nm. MDA kit was derived from Nanjing Jiancheng Bioengineering Institute (Nanjing, China).

ROS Assessment

After $HgCl_2$ and Se treatment, the medium was discarded, and CEK cells were washed with PBS for 3 times. A serum-free medium containing DCFH-DA (Nanjing Jiancheng Bioengineering Institute, Nanjing, China) was then used to treat the cells and incubated for 30 min at 37°C in dark. Subsequently, the residual dye was washed with PBS, and the cells were obtained with a fluorescence microscope.

Intracellular Ca^{2+} Measurement

After $HgCl_2$ and Se treatment, the medium was discarded, and CEK cells were washed with PBS for 3 times. A serum-free medium containing Rhod-2 AM (Nanjing Jiancheng Bioengineering Institute, Nanjing, China) was then used to treat the cells and incubated for 30 min at 37°C in dark. Subsequently, the residual dye was washed with PBS, and the cells were obtained with a fluorescence microscope.

Cell Transfections

MiRNA mimics or inhibitors (Ribobio, Guangzhou, China) were transfected into CEK cells using ribo FECT CP reagent (Ribobio, Guangzhou, China) at a final concentration of 50 or 70 nM according to the manufacturer's instructions. After transfection, cells were cultured in a normal medium for another 24 h or 48 h for the next step. The sequences of miRNA mimics and inhibitors were shown in Table 1.

Plasmid Construction and Dual-luciferase Reporter Assay

To identify the interaction between miR-202-5p and MICU1, the luciferase reporter plasmids PGL4.74 (Syngentech, Beijing, China) inserted with wide type (**wt**) or mutated (**mut**) 3′UTR of MICU1 were constructed. MICU1 wt -3′-UTR or MICU1 mut -3′-UTR with miR-202-5p mimic or miR-202-5p mimic negative control (**NC**) were cotransfected into CEK cells using

Table 1. miRNA sequence in this study.

Primer name	Sequence (5′ to 3′)	Length
gga-miR-202-5p mimic	UUUCCUAUGCAUAUACUUCUUU	22
	AAAGAAGUAUAUGCAUAGGAAA	22
mimic NC	UCACAACCUCCUAGAAAGAGUAGA	24
	UCUACUCUUUCUAGGAGGUUGUGA	24
gga-miR-202-5p inhibitor	AAAGAAGUAUAUGCAUAGGAAA	22
inhibitor NC	UCUACUCUUUCUAGGAGGUUGUGA	24

Lipofectamine 3000 reagent (Invitrogen, Carlsbad, CA). After continuing incubation for 48 h, a dual luciferase reporter kit (Promega, Beijing, China) was used according to the manufacturer's instructions to measure luciferase and renilla activities of these samples. The sequences of MICU1 wt-3'-UTR and MICU1 mut-3'-UTR were shown in Figure 6B.

Total RNA Extraction and Quantitative Real-Time PCR (qRT-PCR)

Total RNA was extracted from kidney tissues and CEK cells with RNAiso Plus (TaKaRa, Tokyo, Japan), and the concentration and purity of total RNA were determined using a Micro Drop ultra-microspectrophotometer (BIO-DL, TX, USA). Complementary DNA (**cDNA**) reverse transcription kit (Roche, Basel, Switzerland) and miRNA First Strand cDNA Synthesis (Tailing Reaction) (Sangon Biotech, Shanghai, China) were used for synthesizing first strand cDNA. All primers were designed and synthesized by Sangon Biotech (Shanghai, China), and their sequences were shown in Table 2. To assess the gene expression levels, the qRT-PCR reaction was performed on LightCycler 96 amplification and detection system (Roche, Basel, Switzerland). The relative expressions of mRNA and miRNA were treated according to the $2^{-\Delta\Delta Ct}$ method.

Western Blot

The total proteins were extracted from kidney tissues and CEK cells, quantified by the Bicinchoninic Acid method, and prepared into protein samples by adding SDS-PAGE protein loading buffer (5 ×) (Beyotime Biotechnology., Shanghai, China). After the samples were treated with 10% SDS-PAGE, protein separated and then were transferred to PVDF membrane. The membranes were subsequently closed with 5% skim milk for 90 min and washed 3 times with TBST. Then incubated with the following primary antibodies (ABclonal, Wuhan, China): GAPDH (1: 10,000 dilution), FPN1, FTH, GPX4, IREB2, MCU, MICU1, phosphorylated mixed lineage kinase domain-like (**P-MLKL**), sodium/calcium exchanger 1 (**NCX1**), receptor-interacting protein kinase 1 (**RIPK1**), FBXL5 (1: 1,000 dilution), receptor-interacting protein kinase 3 (**RIPK3**), and TFRC (1: 3,000 dilution). Membranes were then incubated for 50 min at room temperature in secondary antibodies containing horseradish peroxidase-labeled anti-rabbit IgG or anti-mouse IgG. After washing with TBST, the fluorescence signal was detected using the ECL reagent (Cheml Scope5300, Clinx Science Instruments, Shanghai, China) and the image VCD gel imaging system (Clinx Science Instruments, Shanghai, China).

Table 2. RNA oligonucleotides in this study.

Gene names	Sequence (5′ to 3′)
MICU1	F: CCTCACAACAGTCCTTTCCACTCC
	R: CTTCCATGTCCACTTCACCATCTCC
GAPDH	F: GGTAGTGAAGGCTGCTGCTGATG
	R: AGTCCACAACACGGTTGCTGTATC
MiR-202-5p	F: TTTCCTATGCATATACTTCTTT
U6	F: aggCACGCAAATTCGTGAAGCGTTCCA

Statistical Analysis

The experimental data were statistically analyzed using SPSS 22.0 (Chicago, IL). All data were expressed as mean ± SD (standard deviation). Figures were generated using GraphPad Prism 8.0 software. Comparisons between experimental groups were analyzed by two-way ANOVA. The Scheffe test was used when the data were normally distributed, and the Kruskal-Wallis test was used when the data were not normally distributed. $^{*}P < 0.05$, $^{**}P < 0.01$, ns, not significant.

RESULTS

Se Alleviates $HgCl_2$-induced Chicken Kidney Injury

To explore whether Se can alleviate $HgCl_2$-induced kidney tissue injury, chicken kidney tissues were first observed through histopathological observation. The results showed that the normal cells were round, full, and neatly arranged. However, $HgCl_2$ group showed noticeable pathological changes with destroyed cell membranes (blue arrow), intracellular vacuoles (green arrow), and tissue rupture and decomposition (red arrow). In particular, Se treatment significantly reduced injury with reduced cytoplasmic vacuoles and tissue rupture (Figure 1A). Meanwhile, the content of creatinine (**CREA**), uric acid (**UA**), and carbamide (**UREA**) in chicken serum was measured. These indicators were increased in $HgCl_2$ group significantly, but Se prevented these changes (Figure 1B, $P < 0.01$). The above results suggested that Se could alleviate $HgCl_2$-caused kidney tissue injury.

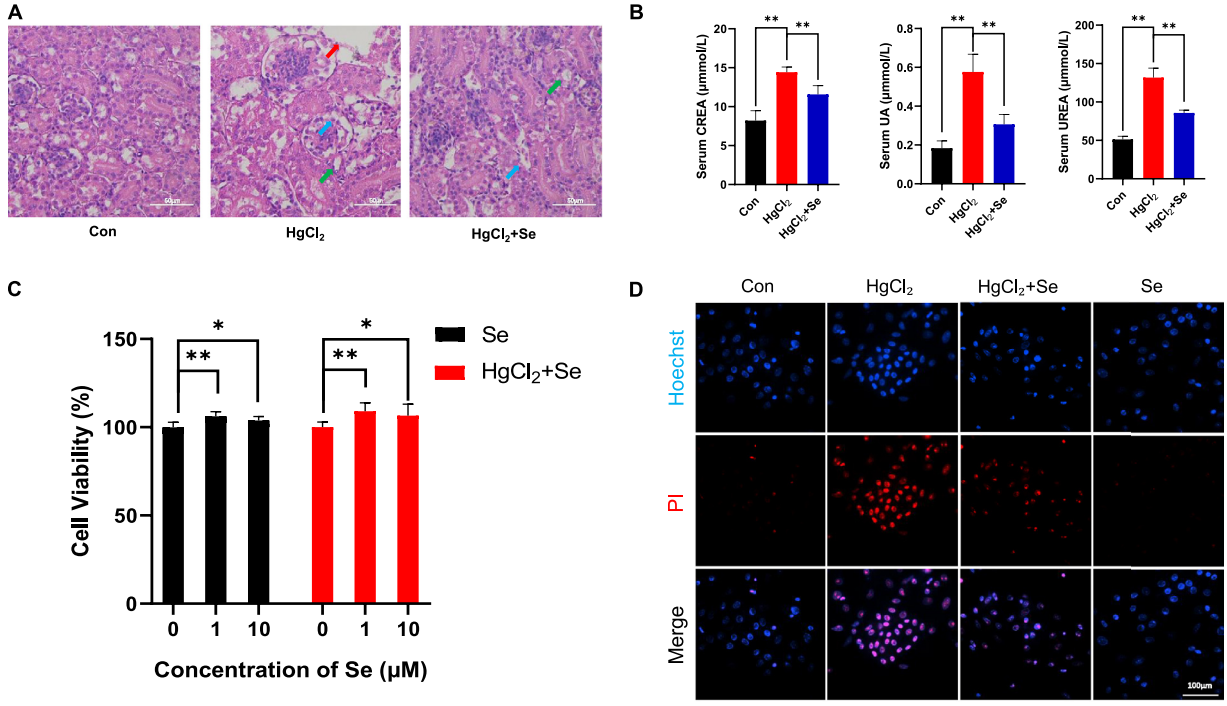

Figure 1. Se alleviates $HgCl_2$-induced kidney injury. (A) Histologically, H&E staining of the kidney was observed. Scale bar = 50 μm. The blue arrows showed destroyed cell membranes; the green arrows showed intracellular vacuoles; the red arrow showed tissue rupture and decomposition. (B) The content of CREA, UA, and UREA was measured in chicken serum using a serum biochemical analyzer. (C) CEK cells were exposed to different concentrations (0, 1, and 10 μM) of Se and $HgCl_2$ (15 μM) for 12 h, and cell viabilities were determined using CCK-8 kit. (D) PI-positive cells were stained using a fluorescence microscope. Scale bar = 100 μm. Significance ($^*P < 0.05$, $^{**}P < 0.01$, ns, not significant). Data represented as mean ± SD (n = 3).

To further investigate whether Se can rescue $HgCl_2$-induced cytotoxicity in CEK cells, an in vitro model of Se antagonism of $HgCl_2$-induced nephrotoxicity was established. The viabilities of CEK cells treated were assayed by CCK-8 assay. The results showed that the toxic effect on cells was minimized when the Se concentration was 1 μM, and in the subsequent experiments, 1 μM was chosen as the Se treatment concentration. Compared to $HgCl_2$ group, the viabilities of cells in $HgCl_2$ + Se group were increased, further indicating that Se mitigated $HgCl_2$-induced kidney cytotoxicity (Figure 1C, $P < 0.05$). Subsequently, the effects of $HgCl_2$ on CEK cells were observed using Hoechst/PI staining (Figure 1D). The results suggested that after $HgCl_2$ treatment, PI reached the nucleus through damaged cell membrane and showed red fluorescence. Moreover, Se significantly inhibited the proliferation of $HgCl_2$-induced PI-positive cells. These results demonstrated that Se had a significant inhibitory effect on $HgCl_2$-induced necrosis.

Se Attenuates $HgCl_2$-Caused Ferroptosis in Chicken Kidneys and CEK Cells

Histopathological changes and Hoechst/PI staining confirmed that $HgCl_2$ caused necrotic changes in the kidney. And it was demonstrated that cells undergoing necroptosis showed characteristics of necrotic cells, such as disruption of cell membranes (Khoury et al., 2020). Therefore, this study investigated whether the damage caused by $HgCl_2$ was due to necroptosis. Necroptosis-related proteins such as RIPK1, P-MLKL, and RIPK3 in kidney tissues (Figures 2A and 2B, $P < 0.05$; ns, not significant) and CEK cells (Figure 2C and 2D, $P < 0.01$; ns, not significant) were detected. RIPK3 protein expression level was increased, while RIPK1, MLKL, and P-MLKL protein expression levels were decreased in $HgCl_2$ group, suggesting that the kidney did not undergo necroptosis.

Ferroptosis acts as a unique form of programmed cell death with a typical necrotic morphology. The appearance of ferroptosis has been reported to be associated with 2 main biochemical characteristics, namely iron overload and lipid peroxidation (Tang et al., 2021). Fe^{2+} is the main factor in ferroptosis, therefore it was tested. As expected, Fe^{2+} levels were significantly increased after $HgCl_2$ exposure and significantly decreased with Se addition (Figure 3A, $P < 0.01$). Next, iron metabolism-related proteins in kidney tissues (Figures 3B and 3C, $P < 0.01$) and CEK cells (Figures 3D and 3E, $P < 0.05$) were examined. The results showed that Se reversed the decrease in the expression levels of IREB2, TFRC, and FTH proteins, and reduced the expression levels of FBXL5 and FPN1 induced by $HgCl_2$, indicating that Se alleviated iron overload caused by $HgCl_2$.

Next, ferroptosis marker protein expression levels were measured. This study found that the expression level of GPX4 protein was significantly reduced in $HgCl_2$ group, consistent with the typical characteristics of ferroptosis. Se reversed the decrease in GPX4

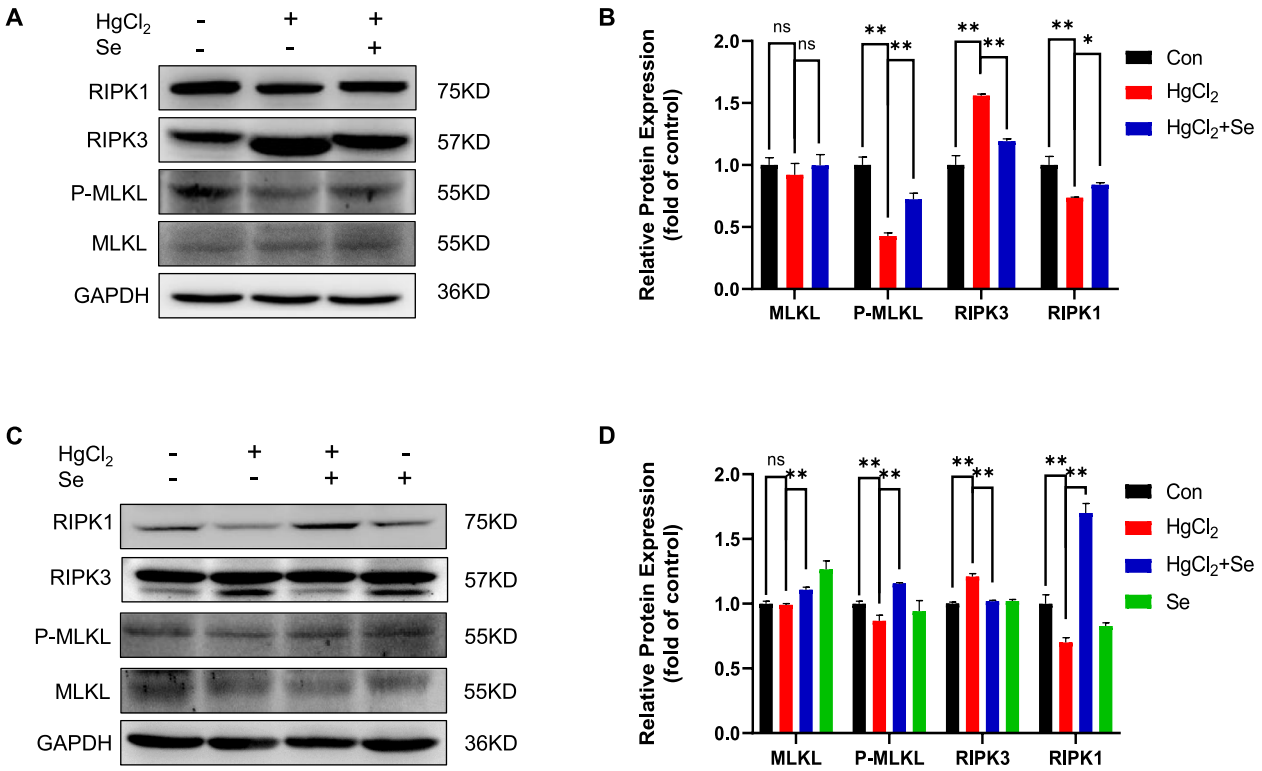

Figure 2. Se alleviates $HgCl_2$-induced death mechanisms excluding necroptosis. (A, B) The protein expressions of RIPK1, RIPK3, MLKL, and P-MLKL in the kidney tissues were determined by Western blot. (C, D) The protein expressions of RIPK1, RIPK3, MLKL, and P-MLKL in CEK cells were determined by Western blot. GAPDH was used as a loading Con. Significance ($^*P < 0.05$, $^{**}P < 0.01$, ns, not significant). Data represented as mean ± SD (n = 3).

expression caused by $HgCl_2$ (Figures 4A and 4B, $P < 0.01$) in chicken kidneys and CEK cells. In addition, the core of ferroptosis is the lethal process of lipid peroxidation. Thus, several indicators of oxidative stress in the kidney tissues were measured. The results demonstrated that Se reversed $HgCl_2$-induced decrease in GSH-Px and T-SOD activities and increase in MDA content, suggesting that Se attenuated the kidney oxidative stress

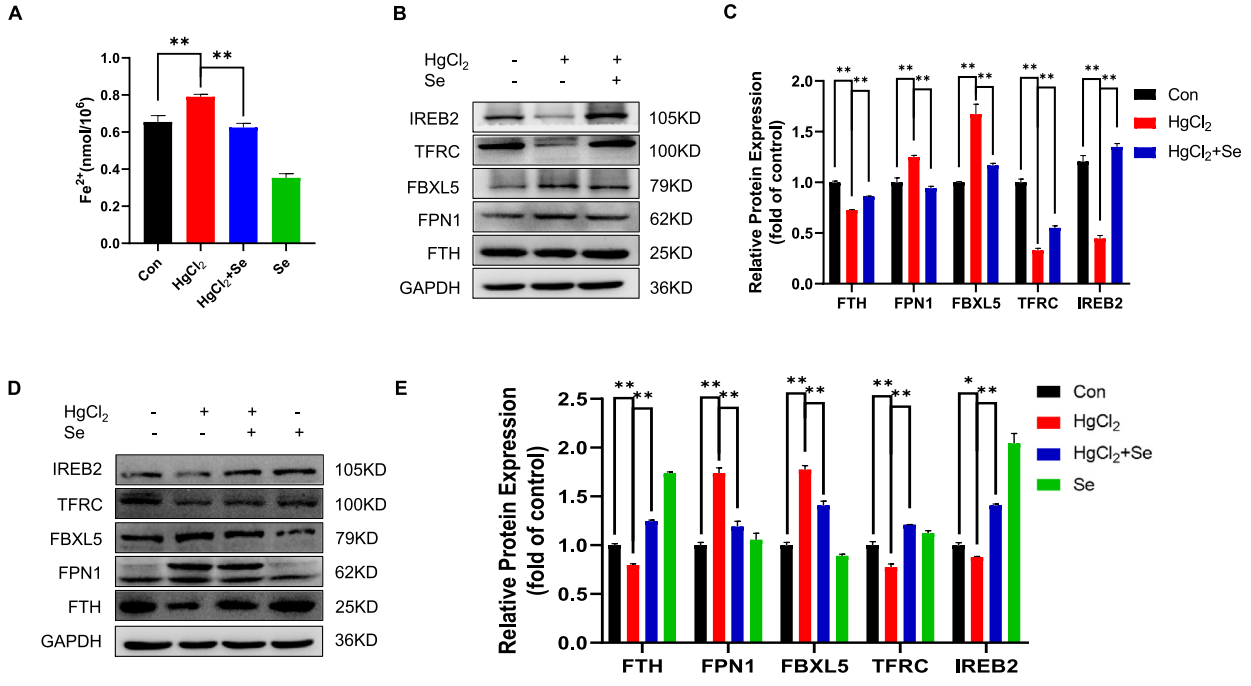

Figure 3. Se attenuates kidney iron overload caused by $HgCl_2$. (A) The level of Fe^{2+} was tested by a commercial kit. (B, C) The protein expressions of IREB2, TFRC, FBXL5, FPN1, and FTH in the kidney tissues were determined by Western blot. (D, E) The protein expressions of IREB2, TFRC, FBXL5, FPN1, and FTH in CEK cells were determined by Western blot. GAPDH was used as a loading Con. Significance ($^*P < 0.05$, $^{**}P < 0.01$, ns, not significant). Data represented as mean ± SD (n = 3).

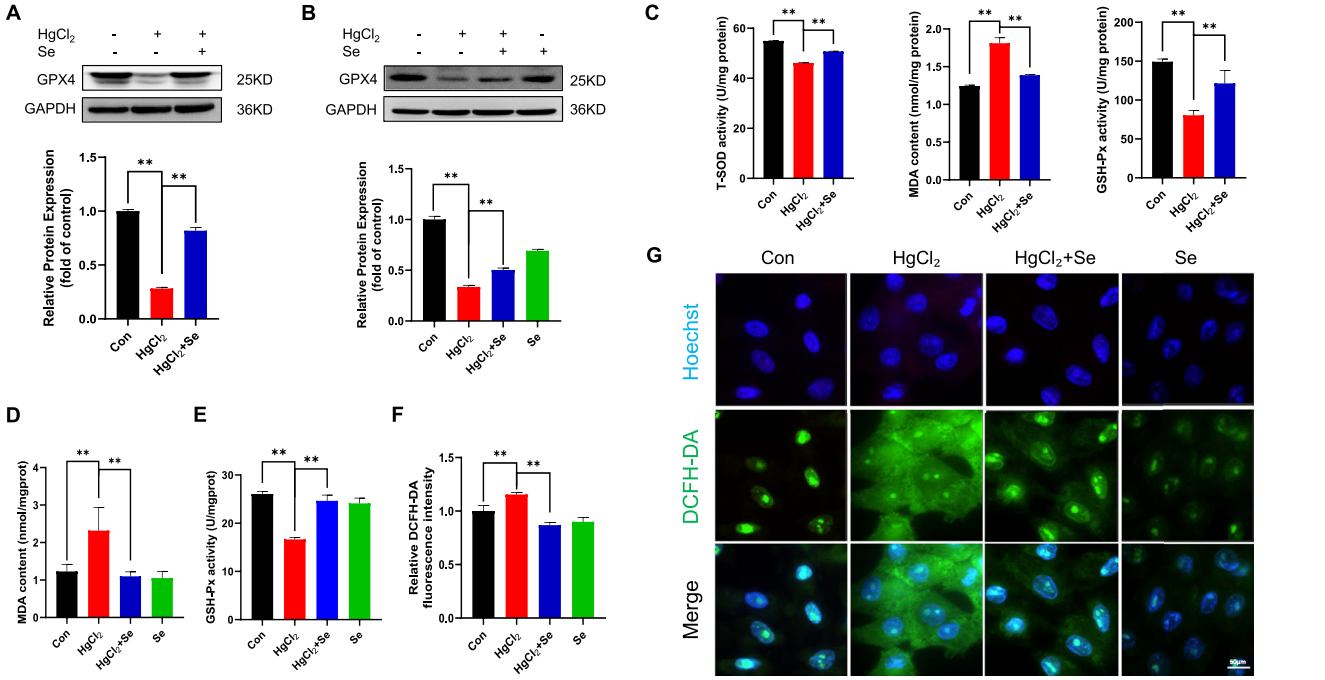

Figure 4. Se attenuates kidney lipid peroxidation caused by $HgCl_2$. (A) The protein expression of GPX4 in the kidney tissues was determined by Western blot. (B) The protein expression of GPX4 in CEK cells was determined by Western blot. GAPDH was used as a loading Con. (C) The content of MDA, and the activities of T-SOD and GSH-Px for the kidney were tested by commercial kits, respectively. (D) The content of MDA in CEK cells was tested by a commercial kit. (E) The activity of GSH-Px in CEK cells was tested by a commercial kit. (F, G) The fluorescence level of DCFH-DA was measured by a fluorescence microscope. Scale bar = 50 μm. Significance ($^*P < 0.05$, $^{**}P < 0.01$, ns, not significant). Data represented as mean ± SD (n = 3).

caused by $HgCl_2$ (Figure 4C, $P < 0.01$). Meanwhile, the content of MDA and the activity of GSH-Px in CEK cells were determined under different treatments (Figures 4D and 4E, $P < 0.01$). In the results, MDA content was increased significantly and GSH-Px activity was decreased significantly in $HgCl_2$ group, and Se supplementation significantly alleviated the changes. Furthermore, DCFH-DA assay was used to detect $HgCl_2$-exposed ROS status in CEK cells (Figures 4F and 4G, $P < 0.01$). Compared with Con group, the ROS levels were significantly higher after $HgCl_2$ exposure, and decreased after Se supplementation. The above results suggested that $HgCl_2$ caused kidney damage by inducing ferroptosis, and Se treatment could alleviate it.

Se Ameliorates $HgCl_2$ Triggered Mitochondrial Ca^{2+} Overload and Increased Mitochondrial ROS in Chicken Kidneys and CEK Cells

Notably, mitochondrial Ca^{2+} has proven to be intimately related to mitochondrial ROS (Baev et al., 2022). First, Ca^{2+} channel-related proteins, such as MCU, MICU1, and NCX1 expression levels were examined in kidney tissues and CEK cells. As shown in the results, MCU protein expression level in $HgCl_2$ group was significantly increased, while MICU1 and NCX1 protein expression levels were considerably decreased, and these changes were reversed in $HgCl_2$ + Se group (Figures 5A−5D, $P < 0.05$). This suggested that $HgCl_2$ had a harmful effect on Ca^{2+} channel-related proteins, resulting in intracellular Ca disturbance, which was mitigated by Se. To further explore the distribution of Ca^{2+} in CEK cells, Ca^{2+} concentrations in mitochondria were measured by Rhod-2 AM fluorescence (Figure 5F). It was shown that Se could effectively attenuate the significant effects of $HgCl_2$ treatment on mitochondrial Ca^{2+} concentrations, further verifying that $HgCl_2$ could trigger mitochondrial Ca^{2+} overload, while Se could ameliorate mitochondrial Ca^{2+} overload.

MiR-202-5p Directly Targets MICU1 and Mediates Mitochondrial Ca^{2+} Overload in CEK Cells

To further identify whether miRNAs are participating in the regulation of MICU1 by $HgCl_2$ and Se, miRDB (http://www.mirdb.org/) and TargetScan (http://www.targetscan.org) 2 genetic biology prediction databases were first used to predict miRNAs targeting MICU1. The results indicated that miR-202-5p was a potential miRNA targeting MICU1, so miR-202-5p was selected as the main target of this study (Figure 6A). Additionally, it was predicted the binding sequence of miR-202-5p and MICU1 (Figure 6B). MICU1 and miR-202-5p gene expression levels in kidney tissues and CEK cells were detected by qRT-PCR and their gene expression levels were negatively correlated (Figures 6C−6F, $P < 0.01$). Moreover, Se reversed the up-regulation of miR-202-5p by $HgCl_2$. Subsequently, the targeting

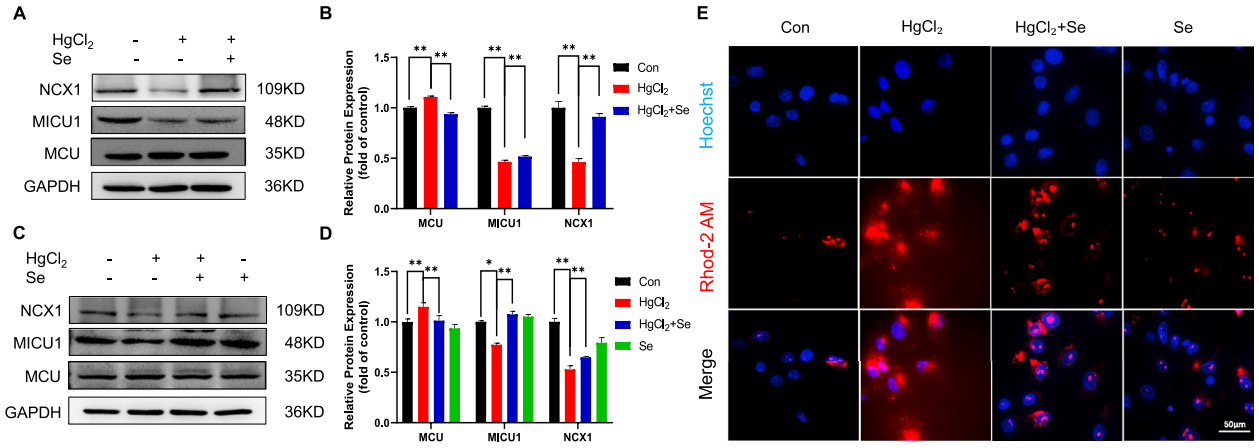

Figure 5. Se ameliorates $HgCl_2$-triggered Ca overload and increased mitochondrial ROS. (A, B) The protein expressions of MCU, MICU1, and NCX1 in the kidney tissues were determined by Western blot. (C, D) The protein expressions of MCU, MICU1, and NCX1 in CEK cells were determined by Western blot. GAPDH was used as a loading Con. (E) Rhod-2 AM fluorescence levels were measured by a fluorescence microscope. Scale bar = 50 μm. Significance ($^*P < 0.05$, $^{**}P < 0.01$, ns, not significant). Data represented as mean ± SD (n = 3).

relationship of miR-202-5p and MICU1 was validated using the dual luciferase reporter gene assay (Figure 6G, $P < 0.01$), and indicated that miR-202-5p mimic efficaciously inhibited the relative luciferase activity of the reporter vector containing MICU1 wt 3′-UTR. MiR-202-5p expression level was significantly increased after miR-202-5p mimic transfection, and decreased after miR-202-5p inhibitor transfection (Figure 6H, $P < 0.01$). Finally, the expression level of MICU1 mRNA was examined. The results showed that MICU1 expression was significantly inhibited or activated after transfection with miR-202-5p mimic or inhibitor (Figure 6I, $P < 0.01$). These results suggested that MICU1 could be directly targeted by miR-202-5p.

Se Antagonizes $HgCl_2$-induced CEK Cell Ferroptosis Mediated by MiR-202-5p Targeting MICU1

After confirming that miR-202-5p targeted MICU1, it was further explored its regulatory role in the mechanism of kidney ferroptosis. First, the Ca^{2+} concentration in mitochondria was examined under different treatment conditions (Figure 7A). As the results showed, the cotreatment of $HgCl_2$ with miR-202-5p inhibitor was able to significantly rescue the increase in mitochondrial Ca^{2+} concentration caused by $HgCl_2$, which was in accordance with the results of $HgCl_2$ + Se group. Similarly, the increased ROS in CEK cells caused by cotreatment

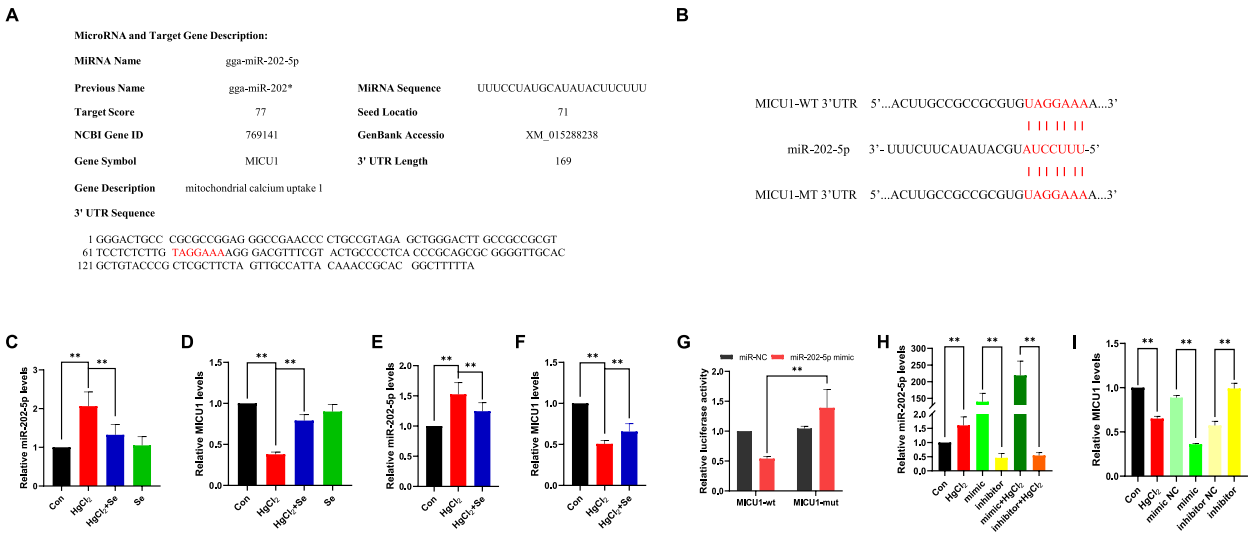

Figure 6. MICU1 is directly targeted by miR-202-5p. (A) The analysis of MICU1 candidate miRNAs including gga-miR-202-5p was performed using the miRDB bioinformatics tool. (B) The binding site between miR-202-5p and MICU1 was predicted by the TargetScan bioinformatics tool. (C-F) The mRNA level of MICU1 and the miRNA level of miR-202-5p were detected in the kidney tissues and CEK cells. (G) Dual-luciferase reporter assays were performed in CEK cells cotransfected with MICU1 mut and miR-202-5p mimic or cotransfected with MICU1 wt and miR-202-5p mimic. (H) The expression level of miR-202-5p was detected after $HgCl_2$ treatment and transfection of miR-202-5p mimic or inhibitor. (I) The expression level of MICU1 was detected after $HgCl_2$ treatment and transfection of miR-202-5p mimic or inhibitor. Significance ($^*P < 0.05$, $^{**}P < 0.01$, ns, not significant). Data represented as mean ± SD (n = 3).

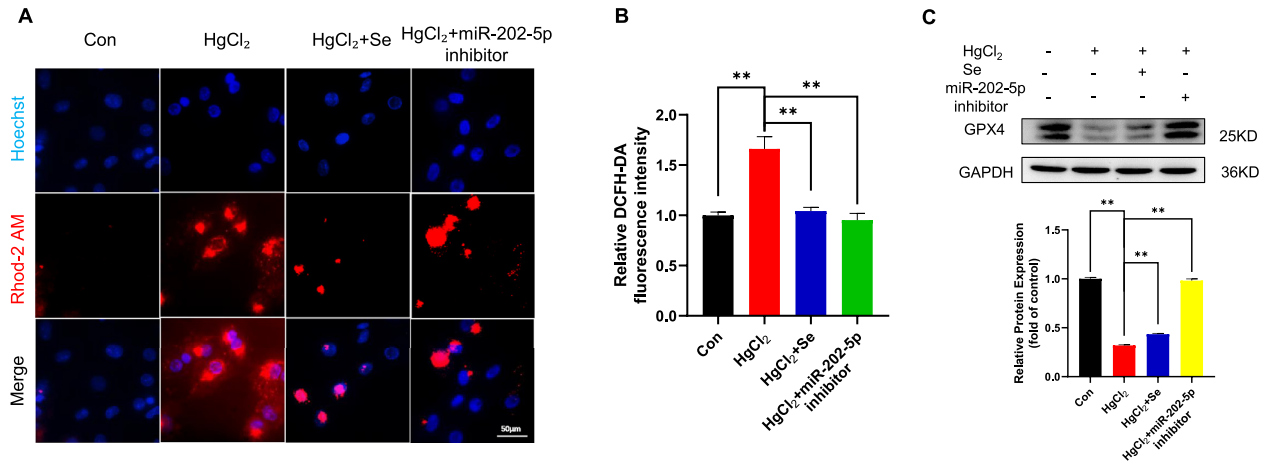

Figure 7. Se antagonizes $HgCl_2$-induced CEK cell ferroptosis mediated by miR-202-5p targeting MICU1. (A) CEK cells were exposed to $HgCl_2$, and $HgCl_2$ with Se or miR-202-5p inhibitor. Rhod-2 AM fluorescence levels were measured by a fluorescence microscope. Scale bar = 50 μm. (B) The fluorescence level of DCFH-DA was measured by a fluorescence microscope. (C) The expression of GPX4 in CEK cells was determined by Western blot. GAPDH was used as a loading Con. Significance ($^*P < 0.05$, $^{**}P < 0.01$, ns, not significant). Data represented as mean ± SD (n = 3).

of $HgCl_2$ with miR-202-5p inhibitor and cotreatment of $HgCl_2$ with Se were significantly alleviated (Figure 7B, $P < 0.01$). Most importantly, in order to investigate the influence of miR-202-5p inhibitor treatment on ferroptosis, ferroptosis marker protein such as GPX4 expression level was examined (Figure 7C, $P < 0.01$). It was observed that the protein expression level of GPX4 was significantly higher after co-treatment of $HgCl_2$ with miR-202-5p inhibitor than that of $HgCl_2$ alone, and $HgCl_2$ + miR-202-5p inhibitor group could obtain similar results as the $HgCl_2$ + Se group. Based on the results obtained above, this study concluded that miR-202-5p mediated the regulation of the ferroptosis pathway in CEK cells by $HgCl_2$ and Se by targeting MICU1.

DISCUSSION

$HgCl_2$ is considered to be one of the most harmful forms of Hg, accumulating in the food chain and having a strong toxic effect on animal organism. There were numerous studies showing that $HgCl_2$ was accumulated in the body and caused damage to the kidney (Li et al., 2019a; Ma et al., 2020). Se supplement was determined to be a potential antagonistic solution to hepatotoxicity induced by heavy metal (Gao et al., 2021). More importantly, Se has the ability to protect multiple types of cells from ferroptosis (Alim et al., 2019). This study was the first to demonstrate that Se antagonized ferroptosis in chicken kidneys caused by $HgCl_2$. Secondly, Se mitigated $HgCl_2$-caused ferroptosis by triggering increased mitochondrial ROS due to Ca^{2+} overload. Thirdly, Se alleviated $HgCl_2$-induced mitochondrial Ca^{2+} overload induced by miR-202-5p mediating MICU1.

The study has shown a strong association between the biological toxicity of $HgCl_2$ and kidney injury (Jiang et al., 2004). In this study, it was observed that exposure to $HgCl_2$ caused typical necrotic changes in the kidney, such as plasma membrane rupture and rupture and decomposition of tissues. Coincidentally, programmed cell death modalities such as necroptosis and ferroptosis, which have been successively discovered in recent years, both cause cell membrane rupture (Pefanis, et al., 2019). Necroptosis is the most typical form of regulatory necrosis that was first studied. The results demonstrated that the levels of necroptosis marker proteins RIPK1 and P-MLKL were reduced after exposure to $HgCl_2$, suggesting that necroptosis might not be the pathway leading to the death of CEK cells. Therefore, an emerging form of necrosis, ferroptosis, was investigated. Importantly, the data showed that $HgCl_2$ exposure resulted in a decrease in GPX4 activity, intracellular iron overload, and lipid peroxidation in kidney tissues and CEK cells, which was the main characteristic of ferroptosis.

A central mechanism of ferroptosis is known to be lipid peroxidation due to ROS and iron overload. What's more, growing instances of ferroptosis targeting mitochondrial ROS have been identified (Zhang, et al., 2020a; Jiang et al., 2022). Next, this study focused on how putative $HgCl_2$ coerces mitochondria to provide essential ROS for ferroptosis. Especially, Ca^{2+} is closely associated with mitochondrial ROS production. Mitochondrial ROS and Ca^{2+} in neurons and astrocytes are physiologically and pathologically regulated by each other, and Ca^{2+} stimulates ROS production (Baev et al., 2022). Notably, mitochondrial Ca^{2+} overload leads to increased mitochondrial ROS production that is independent of the metabolic state of the mitochondria (Görlach et al., 2015). Among these studies, it was demonstrated that $HgCl_2$ exposure caused Ca^{2+} overload in the mitochondria of CEK cells. This was in agreement with the effect of Ca^{2+} overload on ROS, which implied that the increase in mitochondrial ROS due to $HgCl_2$ was caused by mitochondrial Ca^{2+} overload. MCU, a Ca^{2+} selective channel located in the inner mitochondrial membrane, is considered to be the main cause of mitochondrial Ca^{2+}, and its channel activity is regulated by MICU1 (Perocchi et al., 2010; Hempel and Trebak, 2017). NCX1 is the primary pathway of Ca^{2+} efflux in mitochondria, and its reverse mode of operation leads to

mitochondrial Ca^{2+} overload (Lu, et al., 2018). In this study, MICU1 and NCX1 expressions were reduced and MCU expression was increased after $HgCl_2$ treatment. This further added credence to the conclusion that elevated mitochondrial ROS due to $HgCl_2$ was caused by mitochondrial Ca^{2+} overload.

MiR-195 has demonstrated direct targeting of the 3′-UTR of MICU1 mRNA and inhibition of MICU1 expression (Rao et al., 2020). This suggested that miRNA should be further investigated to find miRNAs that interact with MICU1 and it was found that miR-202-5p targeted and acted on MICU1. The previous study has demonstrated that $HgCl_2$ could modulate chicken miRNA expression (Gao et al., 2022). Therefore, whether the regulatory effect of $HgCl_2$ on MICU1 was regulated by miRNAs was further confirmed. The results showed that $HgCl_2$ increased the expression of miR-202-5p and decreased the expression of MICU1, suggesting that miR-202-5p is a bridge connecting $HgCl_2$ and MICU1. Further, the mechanism of ferroptosis due to $HgCl_2$ was investigated, and it was confirmed that $HgCl_2$ could exert toxic effects through miRNAs. More importantly, the targeting relationship among MICU1 and miR-202-5p might be a critical therapeutic target for $HgCl_2$ toxicity.

Se is an effective antagonist of heavy metal toxicity. Previous studies in our group have shown that Se could alleviate $HgCl_2$-caused organ damage (Li et al., 2022a). Recent studies showed that Se inhibited ferroptosis through the specific protein 1/GPX4 pathway (Chen et al., 2022c). Most importantly, the first evidence that Se attenuated the occurrence of signature events of $HgCl_2$-induced ferroptosis was provided by this study. Studies have shown that Se could attenuate necroptosis induced by Cd in the chicken kidney via miR-26a-5p/PTEN/PPI3K/AKT letters (Chen et al., 2021). And previous research has been demonstrated that miR-125a/b played essential roles in the suppression of Cd-induced apoptosis by Se through the mitochondrial pathway (Chen, et al., 2016). Among these results, it was found that the results obtained by treatment with miRNA inhibitor were consistent with those obtained by Se treatment. It implied that miR-202-5p might be a novel mechanism of Se antagonism against $HgCl_2$ toxicity.

In summary, this study showed that Se antagonized $HgCl_2$-induced ferroptosis in chicken kidney. And further studies showed that Se reduced $HgCl_2$-induced ferroptosis in chicken kidney by alleviating mitochondrial Ca^{2+} overload via the miR-202-5p/MICU1 axis. Overall, the present work demonstrated that the miR-202-5p/MICU1 axis could act as a potential emerging target for Se treatment of $HgCl_2$-induced nephrotoxicity.

ACKNOWLEDGMENTS

This work was supported by the National Natural Science Foundation of China [Grant number 32273088, 31902330] and Funds of Shandong "Double Tops" Program.

DISCLOSURES

The authors declare no conflicts of interest.

REFERENCES

Ali, M., X. Zhang, R. LaCanna, D. Tomar, J. W. Elrod, and Y. Tian. 2022. MICU1-dependent mitochondrial calcium uptake regulates lung alveolar type 2 cell plasticity and lung regeneration. JCI Insight 7:e154447.

Alim, I., J. T. Caulfield, Y. Chen, V. Swarup, D. H. Geschwind, E. Ivanova, J. Seravalli, Y. Ai, L. H. Sansing, E. J. Ste Marie, R. J. Hondal, S. Mukherjee, J. W. Cave, B. T. Sagdullaev, S. S. Karuppagounder, and R. R. Ratan. 2019. Selenium Drives a Transcriptional Adaptive Program to Block Ferroptosis and Treat Stroke. Cell 177:1262–1279 e1225.

Avila-Rojas, S. H., A. Lira-León, O. E. Aparicio-Trejo, L. M. Reyes-Fermín, and J. Pedraza-Chaverri. 2019. Role of autophagy on heavy metal-induced renal damage and the protective effects of curcumin in autophagy and kidney preservation. Medicina (Kaunas) 55:360.

Baev, A. Y., A. Y. Vinokurov, I. N. Novikova, V. V. Dremin, E. V. Potapova, and A. Y. Abramov. 2022. Interaction of Mitochondrial Calcium and ROS in Neurodegeneration. Cells 11:706.

Bao, W. D., X. T. Zhou, L. T. Zhou, F. Wang, X. Yin, Y. Lu, L. Q. Zhu, and D. Liu. 2020. Targeting miR-124/Ferroportin signaling ameliorated neuronal cell death through inhibiting apoptosis and ferroptosis in aged intracerebral hemorrhage murine model. Aging Cell 19:e13235.

Bravo-Sagua, R., V. Parra, C. López-Crisosto, P. Díaz, A. F. Quest, and S. Lavandero. 2017. Calcium transport and signaling in mitochondria. Compr. Physiol. 7:623–634.

Caglayan, C., F. M. Kandemir, E. Darendelioğlu, S. Yıldırım, S. Kucukler, and M. B. Dortbudak. 2019. Rutin ameliorates mercuric chloride-induced hepatotoxicity in rats via interfering with oxidative stress, inflammation and apoptosis. J. Trace Elem Med. Biol. 56:60–68.

Chen, H., P. Li, Z. Shen, J. Wang, and L. Diao. 2021. Protective effects of selenium yeast against cadmium-induced necroptosis through miR-26a-5p/PTEN/PI3K/AKT signaling pathway in chicken kidney. Ecotoxicol. Environ. Saf. 220:112387.

Chen, L., C. Liu, Y. Yin, G. Liu, Y. Li, and Y. Cai. 2022a. Mass budget of mercury (Hg) in the seawater of Eastern China marginal seas: importance of the sediment-water transport processes. Environ. Sci. Technol. 56:11418–11428.

Chen, X. W., J. H. Chu, L. X. Li, P. C. Gao, Z. Y. Wang, and R. F. Fan. 2022b. Protective mechanism of selenium on mercuric chloride-induced testis injury in chicken via p38 MAPK/ATF2/iNOS signaling pathway. Theriogenology 187:188–194.

Chen, Y. X., T. Zuliyaer, B. Liu, S. Guo, D. G. Yang, F. Gao, Y. Yu, M. L. Yang, L. J. Du, and J. J. Li. 2022c. Sodium selenite promotes neurological function recovery after spinal cord injury by inhibiting ferroptosis. Neural Regen. Res. 17:2702–2709.

Chen, Z., D. Gu, M. Zhou, H. Shi, S. Yan, and Y. Cai. 2016. Regulatory role of miR-125a/b in the suppression by selenium of cadmium-induced apoptosis via the mitochondrial pathway in LLC-PK1 cells. Chem. Biol. Interact. 243:35–44.

Chu, J. H., L. X. Li, P. C. Gao, X. W. Chen, Z. Y. Wang, and R. F. Fan. 2022. Mercuric chloride induces sequential activation of ferroptosis and necroptosis in chicken embryo kidney cells by triggering ferritinophagy. Free Radic. Biol. Med. 188:35–44.

Chu, J. H., Y. X. Yan, P. C. Gao, X. W. Chen, and R. F. Fan. 2020. Response of selenoproteins gene expression profile to mercuric chloride exposure in chicken kidney. Res. Vet. Sci. 133:4–11.

Ding, C., X. Ding, J. Zheng, B. Wang, Y. Li, H. Xiang, M. Dou, Y. Qiao, P. Tian, and W. Xue. 2020. miR-182-5p and miR-378a-3p regulate ferroptosis in I/R-induced renal injury. Cell Death Dis. 11:929.

Ding, E., J. Guo, Y. Bai, H. Zhang, X. Liu, W. Cai, L. Zhong, and B. Zhu. 2017. MiR-92a and miR-486 are potential diagnostic

biomarkers for mercury poisoning and jointly sustain NF-κB activity in mercury toxicity. Sci. Rep. 7:15980.
Dixon, S. J., K. M. Lemberg, M. R. Lamprecht, R. Skouta, E. M. Zaitsev, C. E. Gleason, D. N. Patel, A. J. Bauer, A. M. Cantley, W. S. Yang, B. Morrison 3rd, and B. R. Stockwell. 2012. Ferroptosis: an iron-dependent form of non-apoptotic cell death. Cell 149:1060–1072.
Fan, R. F., J. X. Liu, Y. X. Yan, L. Wang, and Z. Y. Wang. 2020. Selenium relieves oxidative stress, inflammation, and apoptosis within spleen of chicken exposed to mercuric chloride. Poult. Sci. 99:5430–5439.
Fuhrmann, D. C., A. Mondorf, J. Beifuß, M. Jung, and B. Brüne. 2020. Hypoxia inhibits ferritinophagy, increases mitochondrial ferritin, and protects from ferroptosis. Redox Biol. 36:101670.
Gao, P. C., X. W. Chen, J. H. Chu, L. X. Li, Z. Y. Wang, and R. F. Fan. 2022. Antagonistic effect of selenium on mercuric chloride in the central immune organs of chickens: the role of microRNA-183/135b-FOXO1/TXNIP/NLRP3 inflammasome axis. Environ Toxicol 37:1047–1057.
Gao, P. C., J. H. Chu, X. W. Chen, L. X. Li, and R. F. Fan. 2021. Selenium alleviates mercury chloride-induced liver injury by regulating mitochondrial dynamics to inhibit the crosstalk between energy metabolism disorder and NF-κB/NLRP3 inflammasome-mediated inflammation. Ecotoxicol. Environ. Saf. 228:113018.
Görlach, A., K. Bertram, S. Hudecova, and O. Krizanova. 2015. Calcium and ROS: a mutual interplay. Redox Biol 6:260–271.
Hao, S., B. Liang, Q. Huang, S. Dong, Z. Wu, W. He, and M. Shi. 2018. Metabolic networks in ferroptosis. Oncol Lett 15:5405–5411.
Hazelhoff, M. H., and A. M. Torres. 2018. Gender differences in mercury-induced hepatotoxicity: potential mechanisms. Chemosphere 202:330–338.
Hempel, N., and M. Trebak. 2017. Crosstalk between calcium and reactive oxygen species signaling in cancer. Cell Calcium 63:70–96.
Hosseini, A., A. Rajabian, S. Fanoudi, M. Farzadnia, and M. T. Boroushaki. 2018. Protective effect of Rheum turkestanicum root against mercuric chloride-induced hepatorenal toxicity in rats. Avicenna J. Phytomed. 8:488–497.
Hu, W., Y. Yu, Y. Sun, F. Yuan, and F. Zhao. 2022. MiR-25 overexpression inhibits titanium particle-induced osteoclast differentiation via down-regulation of mitochondrial calcium uniporter in vitro. J. Orthop. Surg. Res. 17:133.
Jiang, J., D. Dean, R. C. Burghardt, and A. R. Parrish. 2004. Disruption of cadherin/catenin expression, localization, and interactions during HgCl2-induced nephrotoxicity. Toxicol. Sci. 80:170–182.
Jiang, J. J., G. F. Zhang, J. Y. Zheng, J. H. Sun, and S. B. Ding. 2022. Targeting mitochondrial ROS-mediated ferroptosis by quercetin alleviates high-fat diet-induced hepatic lipotoxicity. Front. Pharmacol. 13:876550.
Khoury, M. K., K. Gupta, S. R. Franco, and B. Liu. 2020. Necroptosis in the pathophysiology of disease. Am. J. Pathol. 190:272–285.
Latunde-Dada, G. O. 2017. Ferroptosis: role of lipid peroxidation, iron and ferritinophagy. Biochim. Biophys. Acta Gen. Subj. 1861:1893–1900.
Li, L. X., J. H. Chu, X. W. Chen, P. C. Gao, Z. Y. Wang, C. Liu, and R. F. Fan. 2022a. Selenium ameliorates mercuric chloride-induced brain damage through activating BDNF/TrKB/PI3K/AKT and inhibiting NF-κB signaling pathways. J. Inorg. Biochem. 229:111716.
Li, M. D., L. Fu, B. B. Lv, Y. Xiang, H. X. Xiang, D. X. Xu, and H. Zhao. 2022b. Arsenic induces ferroptosis and acute lung injury through mtROS-mediated mitochondria-associated endoplasmic reticulum membrane dysfunction. Ecotoxicol. Environ. Saf. 238:113595.
Li, S., R. Baiyun, Z. Lv, J. Li, D. Han, W. Zhao, L. Yu, N. Deng, Z. Liu, and Z. Zhang. 2019a. Exploring the kidney hazard of exposure to mercuric chloride in mice:Disorder of mitochondrial dynamics induces oxidative stress and results in apoptosis. Chemosphere 234:822–829.
Li, S., X. Jiang, Y. Luo, B. Zhou, M. Shi, F. Liu, and A. Sha. 2019b. Sodium/calcium overload and Sirt1/Nrf2/OH-1 pathway are critical events in mercuric chloride-induced nephrotoxicity. Chemosphere 234:579–588.
Liang, L., K. Huang, W. Yuan, L. Liu, F. Zou, and G. Wang. 2021. Dysregulations of miR-503-5p and Wnt/β-catenin pathway coordinate in mediating cadmium-induced kidney fibrosis. Ecotoxicol. Environ. Saf. 224:112667.
Lu, Z., Y. Cui, X. Wei, P. Gao, H. Zhang, X. Wei, Q. Li, F. Sun, Z. Yan, H. Zheng, G. Yang, D. Liu, and Z. Zhu. 2018. Deficiency of PKD2L1 (TRPP3) exacerbates pathological cardiac hypertrophy by augmenting NCX1-mediated mitochondrial calcium overload. Cell Rep. 24:1639–1652.
Ma, Y., Y. Shi, L. Li, C. Xie, and X. Zou. 2018. Toxicological effects of mercury chloride on laying performance, egg quality, serum biochemistry, and histopathology of liver and kidney in laying hens. Biol. Trace Elem. Res. 185:465–474.
Ma, Y., Y. Shi, X. Zou, Q. Wu, and J. Wang. 2020. Apoptosis induced by mercuric chloride is associated with upregulation of PERK-ATF4-CHOP pathway in chicken embryonic kidney cells. Poult. Sci. 99:5802–5813.
Paupe, V., and J. Prudent. 2018. New insights into the role of mitochondrial calcium homeostasis in cell migration. Biochem. Biophys. Res. Commun. 500:75–86.
Pefanis, A., F. L. Ierino, J. M. Murphy, and P. J. Cowan. 2019. Regulated necrosis in kidney ischemia-reperfusion injury. Kidney Int. 96:291–301.
Perocchi, F., V. M. Gohil, H. S. Girgis, X. R. Bao, J. E. McCombs, A. E. Palmer, and V. K. Mootha. 2010. MICU1 encodes a mitochondrial EF hand protein required for Ca(2+) uptake. Nature 467:291–296.
Rao, G., S. K. D. Dwivedi, Y. Zhang, A. Dey, K. Shameer, R. Karthik, S. Srikantan, M. N. Hossen, J. D. Wren, M. Madesh, J. T. Dudley, R. Bhattacharya, and P. Mukherjee. 2020. MicroRNA-195 controls MICU1 expression and tumor growth in ovarian cancer. EMBO Rep 21:e48483.
Tang, D., X. Chen, R. Kang, and G. Kroemer. 2021. Ferroptosis: molecular mechanisms and health implications. Cell Res 31:107–125.
Wang, H., H. Shi, M. Rajan, E. R. Canarie, S. Hong, D. Simoneschi, M. Pagano, M. F. Bush, S. Stoll, E. A. Leibold, and N. Zheng. 2020. FBXL5 regulates IRP2 stability in iron homeostasis via an oxygen-responsive [2Fe2S] cluster. Mol Cell 78:31–41 e35.
Yang, D., Q. Yang, N. Fu, S. Li, B. Han, Y. Liu, Y. Tang, X. Guo, Z. Lv, and Z. Zhang. 2021. Hexavalent chromium induced heart dysfunction via Sesn2-mediated impairment of mitochondrial function and energy supply. Chemosphere 264:128547.
Yang, Y., J. Du, R. Xu, Y. Shen, D. Yang, D. Li, H. Hu, H. Pei, and Y. Yang. 2020. Melatonin alleviates angiotensin-II-induced cardiac hypertrophy via activating MICU1 pathway. Aging (Albany NY) 13:493–515.
Zhang, H., T. Deng, R. Liu, T. Ning, H. Yang, D. Liu, Q. Zhang, D. Lin, S. Ge, M. Bai, X. Wang, L. Zhang, H. Li, Y. Yang, Z. Ji, H. Wang, G. Ying, and Y. Ba. 2020a. CAF secreted miR-522 suppresses ferroptosis and promotes acquired chemo-resistance in gastric cancer. Mol. Cancer 19:43.
Zhang, J., S. Zheng, S. Wang, Q. Liu, and S. Xu. 2020b. Cadmium-induced oxidative stress promotes apoptosis and necrosis through the regulation of the miR-216a-PI3K/AKT axis in common carp lymphocytes and antagonized by selenium. Chemosphere 258:127341.
Zhang, Y., R. V. Swanda, L. Nie, X. Liu, C. Wang, H. Lee, G. Lei, C. Mao, P. Koppula, W. Cheng, J. Zhang, Z. Xiao, L. Zhuang, B. Fang, J. Chen, S. B. Qian, and B. Gan. 2021. mTORC1 couples cyst(e)ine availability with GPX4 protein synthesis and ferroptosis regulation. Nat Commun 12:1589.
Zheng, Y., H. Guan, J. Yang, J. Cai, Q. Liu, and Z. Zhang. 2021. Calcium overload and reactive oxygen species accumulation induced by selenium deficiency promote autophagy in swine small intestine. Anim Nutr 7:997–1008.
Zhou, C., P. Xu, C. Huang, G. Liu, S. Chen, G. Hu, G. Li, P. Liu, and X. Guo. 2020. Effects of subchronic exposure of mercuric chloride on intestinal histology and microbiota in the cecum of chicken. Ecotoxicol Environ Saf 188:109920.